Study of one-dimensional spectral dynamic equations of the Reynolds stresses in homogeneous anisotropic turbulence: Application to split-spectrum modeling

By R. Schiestel[1]

The CTR numerical data base generated by direct simulation of homogeneous anisotropic turbulence has been used to calculate all of the terms in the spectral balance equations for the turbulent Reynolds stresses. The aim is not only to test the main closure assumptions used in the split-spectrum model, but also to try to devise improved hypotheses deduced from the statistical information.

1. Description of the Split-Spectrum Model

1.1 Framework

The split-spectrum approach is a very simple way to introduce some spectral information into one-point closure formalisms. The starting point is the spectral equation for the Reynolds stress tensor $\Phi_{ij}(\mathbf{k})$ originating from equations for the two-point velocity correlations. The one-dimensional spectral equations are then obtained by spherical integration in Fourier space. The split-spectrum scheme is developed (Launder & Schiestel 1978, and Schiestel 1987) on the basis of partial integration of the spectral equations over wavenumber intervals. The transport equations for the partial stresses (figure 1) can be written formally:

$$\frac{dR_{ij}^{(m)}}{dt} = \underbrace{P_{ij}^{(m)}}_{A} + \underbrace{F_{ij}^{(m-1)} - F_{ij}^{(m)}}_{B} + \underbrace{\Psi_{ij}^{(m)}}_{C} - \underbrace{D_{ij}^{(m)}}_{D} \quad , \tag{1}$$

where

$$R_{ij}^{(m)} = \int_{k_{m-1}}^{k_m} \varphi_{ij}(k)dk, \qquad \text{and} \qquad \varphi_{ij}(k) = \oint \Phi_{ij}(\mathbf{k})dA(k). \tag{2}$$

This multiple component splitting is such that the usual Reynolds stress R_{ij} is given by

$$R_{ij} = \sum_{m=1}^{M} R_{ij}^{(m)}. \tag{3}$$

The different terms on the right side of (1) represent the following processes in spectral slice m:

1 Institut de Mecanique Statistique de la Turbulence

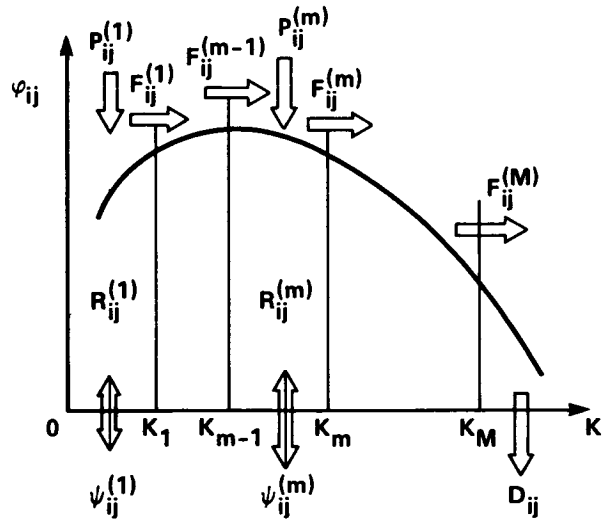

FIGURE 1. Decomposition of wave space into discrete slices.

A) production of $R_{ij}^{(m)}$ by mean velocity gradients;
B) net turbulent flux into the slice including inertial cascade transfer, transfer due to mean strain, and the effect of time varying k_m;

$$F_{ij} = {}_N F_{ij} + {}_L F_{ij} - \varphi_{ij} \frac{\partial k_m}{\partial t}$$

C) redistribution by pressure-velocity correlations including the fast and slow parts;
D) viscous dissipation.

The definition of the time varying wavenumbers k_m, which is related to the energy spectrum, and the hypotheses on energy transfer across the spectrum are used to derive transport equations for the energy flux $F = \frac{1}{2} F_{jj}$. In practical applications M is usually 2 or 3 but here, for the purpose of testing hypotheses, we consider the wavenumber intervals given by the discrete mesh of the simulation.

1.2 Hypotheses

All of the main closure hypotheses can be tested by using the simulation data. These are:

- rapid pressure-strain term:
  The relaxation-of-production approximation is

$$ {}_L\Psi_{ij}^{(m)} \approx -C_2 (P_{ij}^{(m)} - \frac{P_{ll}^{(m)}}{3} \delta_{ij}) \tag{4}$$

- slow pressure-strain term:

The local-return-to-isotropy approximation is

$$ {}_N\Psi_{ij}^{(m)} \approx -C_1 \frac{\epsilon}{K}(R_{ij}^{(m)} - \frac{R_{ll}^{(m)}}{3}\delta_{ij}) \tag{5} $$

Although this looks like Rotta's model, the behavior can be very different.

- inertial transfer of energy:
  The Kovasznay model for the transfer of energy is

$$ {}_N\mathcal{F} \approx \gamma_K \mathcal{E}^{3/2} k^{5/2} \tag{6} $$

  where $\mathcal{E}(k) = \frac{1}{2}\varphi_{jj}(k)$
- energy transfer due to mean strain, $\Lambda_{ij} = \partial\overline{u_i}/\partial x_j$:

$$ {}_L\mathcal{F} \approx -\frac{2k}{5}\varphi_{ij}\Lambda_{ij} \tag{7} $$

- slow transfer for stress components:

$$ {}_NF_{ij} \approx {}_N\mathcal{F}(a\frac{\varphi_{ij}}{\mathcal{E}} + \frac{2(1-a)}{3}\delta_{ij}) \tag{8} $$

- rapid transfer for stress components:
  A proposal of D. Jeandel and J. Mathieu is

$$ {}_LF_{ij} \approx \frac{k}{20}[\varphi_{li}(\Lambda_{lj}+\Lambda_{jl}) + \varphi_{lj}(\Lambda_{li}+\Lambda_{il})] - \frac{k}{5}\varphi_{lm}\Lambda_{lm}\delta_{ij} \tag{9} $$

These closure hypotheses are among the simplest ones that can be formulated. Our goal is to use the results of the simulations to determine the accuracy of these models and, when the models must be improved, to suggest the form of more sophisticated approximations.

2. Use of the simulation data

2.1 Methodology

The simulation database provides the Fourier transform of the velocity field $\widehat{u}_i(\mathbf{k})$ for one realization of the flow field. The equation for the Reynolds stress spectrum tensor $\Phi_{ij}(\mathbf{k}) \equiv \widehat{u}_i(\mathbf{k})\widehat{u}_j(-\mathbf{k})$ can be written in terms of velocity Fourier modes:

$$ \frac{\partial\Phi_{ij}}{\partial t} + \underbrace{\Lambda_{il}\Phi_{lj} + \Lambda_{jl}\Phi_{il}}_{P_{ij}} - \underbrace{\frac{2\Lambda_{lm}k_l}{k^2}(k_i\Phi_{mj} + k_j\Phi_{im})}_{{}_L\Pi_{ij}} - \underbrace{\Lambda_{lm}\frac{\partial}{\partial k_m}(k_l\Phi_{ij})}_{{}_LT_{ij}} $$

$$ \underbrace{- \frac{ik_mk_l}{k^2}[k_i\widehat{u}_j(-\mathbf{k})\widehat{u_lu_m}(\mathbf{k}) - k_j\widehat{u}_i(\mathbf{k})\widehat{u_lu_m}(-\mathbf{k})]}_{{}_N\Pi_{ij}} $$

$$ + \underbrace{ik_m[\widehat{u}_j(-\mathbf{k})\widehat{u_iu_m}(\mathbf{k}) - \widehat{u}_i(\mathbf{k})\widehat{u_ju_m}(-\mathbf{k})]}_{{}_NT_{ij}} + \underbrace{2\nu k^2\Phi_{ij}}_{\epsilon_{ij}} = 0 \tag{10} $$

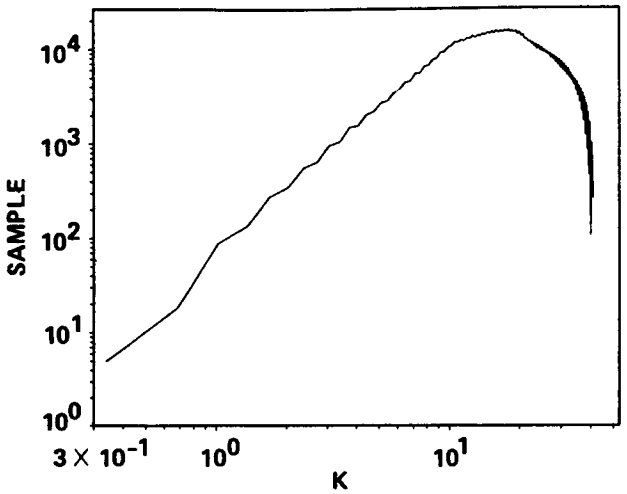

FIGURE 2. Typical variation of statistical sample with scale. Case PXB4 is shown.

One-dimensional spectra are then obtained by summing over the sample within spherical shells. Thus we readily get the necessary terms to test hypotheses (4) to (9).

$$\begin{aligned} R_{ij}^{(m)} &= \sum_{(m)} \Phi_{ij} \quad {}_N\Psi_{ij}^{(m)} = \sum_{(m)} {}_N\Pi_{ij} \quad {}_NF_{ij}^{(m)} = \sum_{(m)} {}_NT_{ij} \\ P_{ij}^{(m)} &= \sum_{(m)} p_{ij} \quad {}_L\Psi_{ij}^{(m)} = \sum_{(m)} {}_L\Pi_{ij} \quad {}_LF_{ij}^{(m)} = \sum_{(m)} {}_LT_{ij} \end{aligned} \tag{11}$$

This treatment has been carried out using an adaptation of Rogallo's (1981) computer code. The program computes the balance of each component of the Reynolds stress spectrum tensor, the sums (11), and performs the comparisons (4) to (9) using flow fields from the stored database.

The transfer term, ${}_LT_{ij}$ in (10), is difficult to compute because derivatives with respect to wavenumber can not be accurately calculated within the context of the simulation. In the simulation, a coordinate system moving with the mean flow was used to remove such derivatives. The problem of evaluating ${}_LT_{ij}$ has been avoided by considering the gross flux ${}_LF_{ij}$. Using

$$\int {}_LT_{ij} d\mathbf{k} = \oint \Lambda_{lm} \frac{k_l k_m}{k} \Phi_{ij} dA(k)$$

we find

$${}_LF_{ij}^{(m)} = \frac{1}{\delta k} \sum_{(m)} \Lambda_{ln} \frac{k_l k_n}{k} \Phi_{ij}$$

The simulation shell sample varies with wave number (figure 2). For low wave numbers the sample increases as k^2 (spherical shell), but due to the anisotropy of the wave-space grid the sample decreases at high wave numbers even before the limit of resolution is reached. In this case, we do not obtain true spherical averages because some directions are privileged.

2.2 Test cases.

In order to reach some degree of generality, it is necessary to consider a number of different flows. The following test cases from the CTR database have been considered:

uniform shear
RR1288
isotropic decay
HIE1
simple strains and relaxation from them
HIA9 PXB4 B4R1 B4R6 (plane strain)
HIC6 AXL6 L6R1 L6R6 (axisymmetric contraction)
HID6 P6R1 P6R6 (axisymmetric expansion)
successive strains and relaxation from them
M2V1 M2V1R1 M2V1R5
K3V1 K3V1R1 K3V1R5
M2U1 M2U1R1 M2U1R5

The shear case is from Rogers et al (1986) and the remaining fields are from Lee & Reynolds (1985).

3 Comparisons and discussion

3.1 Homogeneous shear

The spectra of the various terms in the transport equation for $\overline{u^2}$ are shown in figure 3a. All of the terms have been filtered using a $(\frac{1}{4}, \frac{1}{2}, \frac{1}{4})$ molecule to reduce noise, however the rapid transfer term remains rather noisy.

Figure 3b compares the gross-flux, linear "fast" part and non-linear "slow" part to their approximations given by (6) and (7). The Kovasznay hypothesis overestimates the non-linear transfer (possibly due to the lack of an inertial range in the simulation). The free model constants are taken as unity here and in the following figures and we direct our attention to how well the spectral shape of the model conforms to that of the modelled term. All values are normalized using the appropriate powers of kinetic energy and dissipation rate.

The fast pressure term and the slow pressure term are compared in figure 3c to their approximations given by (4) and (5). The results are encouraging.

The linear transfer is overestimated by (9), but the sign of the approximation is generally correct and the shape of the curve is acceptable. The model (8) for the slow-transfer tensor approximation, with $a = 1$, is often nearly satisfied. This is illustrated for the $\overline{u^2}$ component in figure 3d. Figure 3e shows the ratio of the right side of (4) to the left side and can be interpreted as the variation of C_2 with wavenumber and with stress component. The jumps simply reflect the fact that the zero crossings of the data are not predicted exactly by the model. For components $\overline{u^2}$, $\overline{v^2}$, $\overline{w^2}$, and $\overline{uv}$ the mean value of $C_2 = 0.6$ that is frequently used in classical one-point closure can be inferred. The same ratio for (5) is presented in figure 3f. We see that the coefficient C_1 increases continuously with k, implying a more rapid return to isotropy at high wavenumbers.

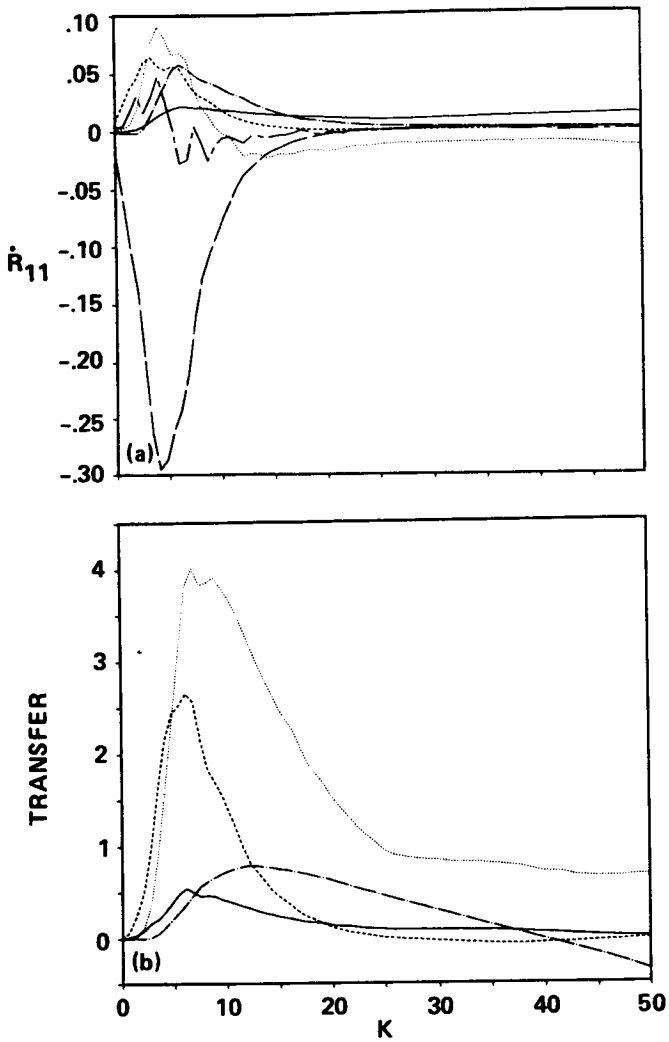

FIGURE 3. Homogeneous shear turbulence. Case RR1288 is shown. (a): budget for R_{11}; ---- production, ---- fast pressure-strain, — · — slow pressure-strain, — - — fast transfer, ····· slow transfer, —— dissipation. (b): gross energy transfer, fast part; —— data, ---- model (7), slow part; — · — data, ····· model (6).

3.2 Simple strains.

Comparisons like those above are presented in figures 4a to 4d for the case of a plane strain. The models for the pressure terms compare favorably, but the model (8) seems inadequate for the slow transfer terms. Similiarly, the model (6) overestimates the nonlinear transfer of energy. The coefficients C_1 and C_2 both increase slowly with k and are different for each component of the tensor.

3.3 Successive strains and relaxation

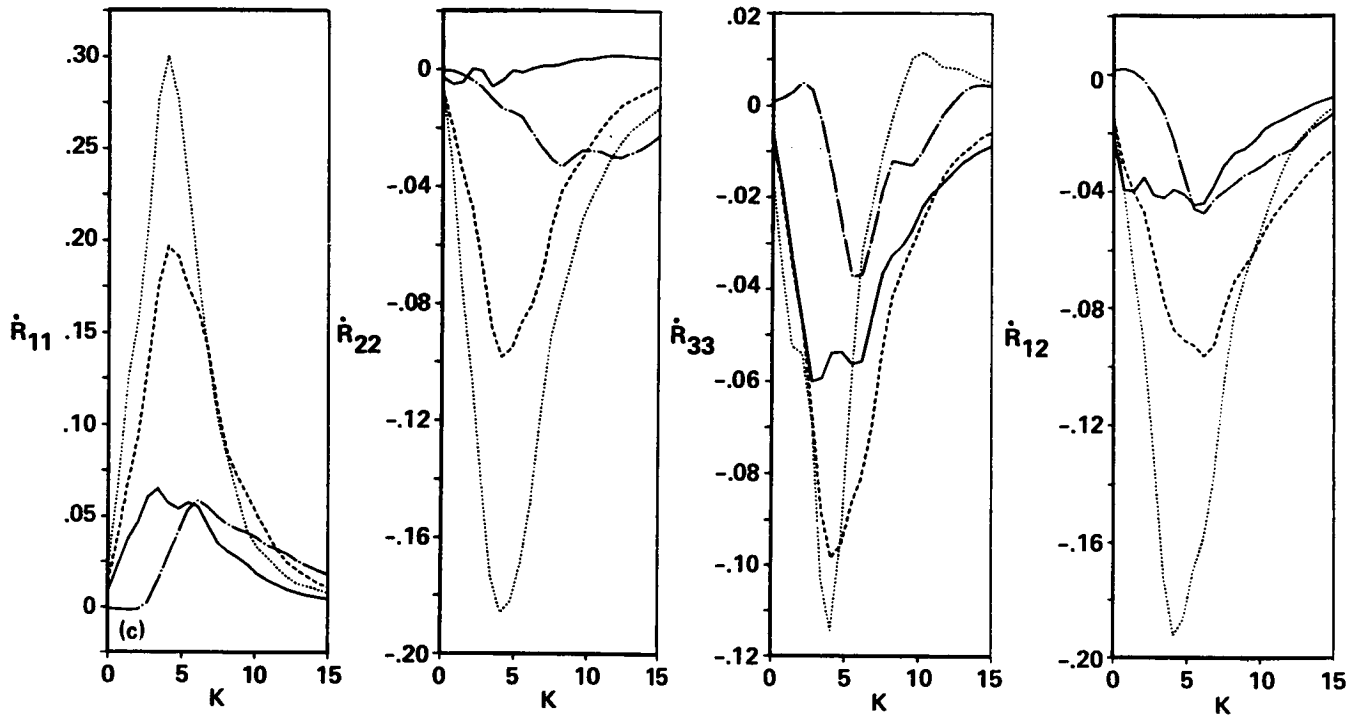

FIGURE 3 (CONTINUED). (c): pressure-strain terms, fast part; —— data, - - - - model (4), slow part; — · — data, ····· model (5).

This is an interesting case and is particularly relevant for the multiple-scale approach. The M2V1 flow (figure 5) is the result of a strong axisymmetric contraction followed by a plane strain. The M2V1R1 flow (figure 6) is the relaxation of M2V1 when the straining ceases. Most of the remarks in section 3.2 are still applicable. In this particular case the simulation exhibits an increase of the Reynolds stress anisotropy at the beginning of decay. This paradoxical effect can be produced by (5) when the coefficient C_1 increases with wavenumber (this occurs for example in figure 6b) and when the initial spectral distribution is such that anisotropies at large and small scales are more or less compensating (this occurs in M2V1). Then a rapid return to isotropy of the fine scales reveals the anisotropy of the larger scales which was hidden temporarily (Schiestel 1986). Such a behavior cannot be obtained with one-point models using the Rotta hypothesis. Some spectral information is necessary to describe this phenomenon.

4. Concluding remarks.

Numerical simulations of turbulent flows provide a large amount of data, a thought provoking wealth of information.

The main advantage of this type of comparison is that a great variety of flows can be considered, and this is necessary to test closure hypotheses. Moreover various

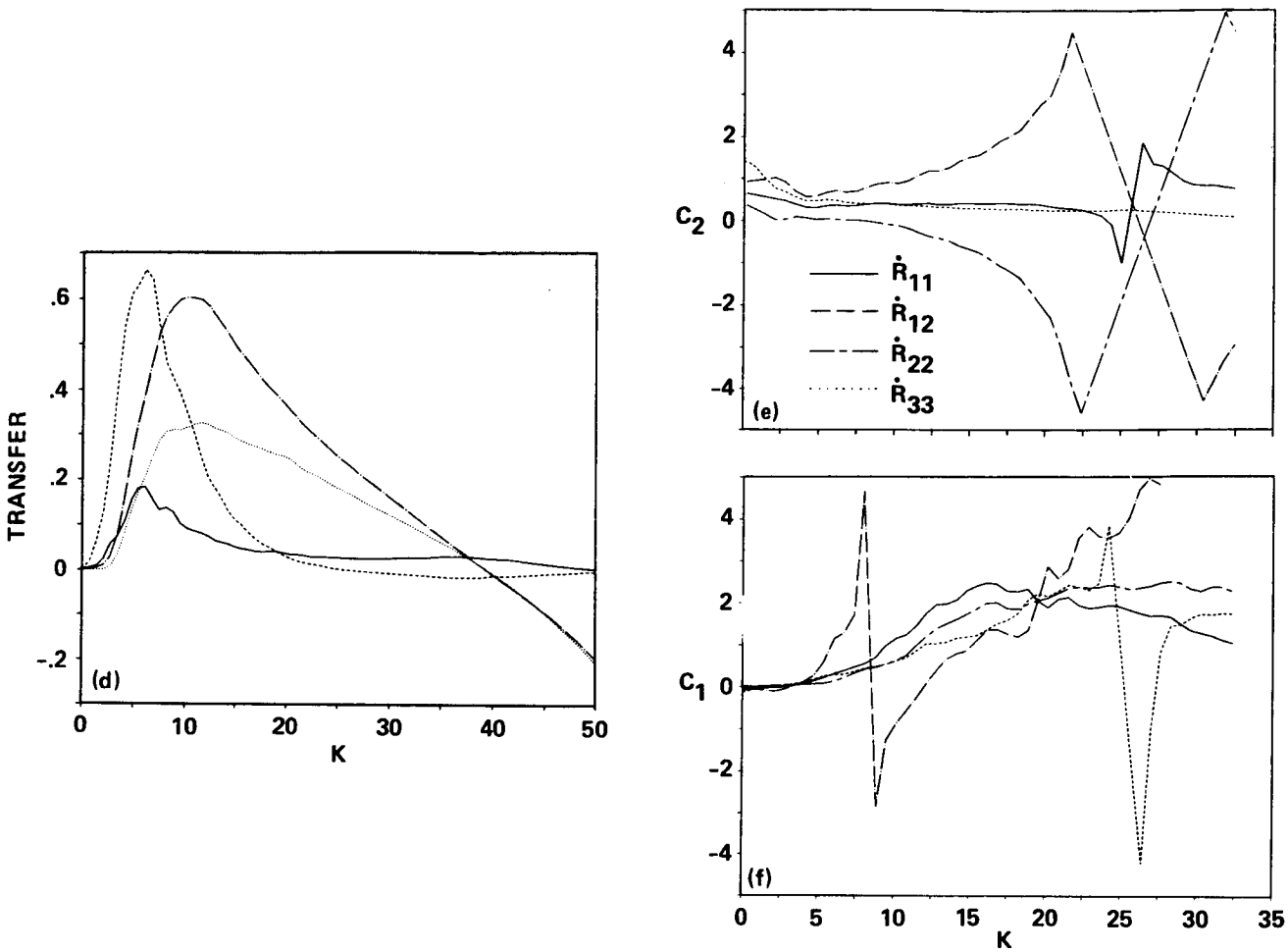

FIGURE 3 (CONCLUDED). (d): gross transfer of R_{11}, fast part; —— data, - - - - model (9), slow part; — · — data, ····· model (8). Variation of the pressure-strain model coefficients for each component of R_{ij}: (e) fast part, (f) slow part.

initial conditions can be introduced in the calculation, even if they are not experimentally feasible. Various statistical information can be easily extracted from the data. All the terms in the spectral equations can be calculated, and this is particularly interesting for terms involving pressure correlations that cannot be measured. The limited Reynolds numbers of the simulations and the statistical noise caused by a small sample, particularly at the large scales, causes some difficulty in the interpretation of the results, but the method of approach proved to be a powerful tool for testing and improving spectral closures.

REFERENCES

LAUNDER, B.E. AND SCHIESTEL, R. 1978 *C.R. Academy of Science, Paris.* **t. 286, ser A,** 709-712.

SCHIESTEL, R. 1987 *Phys. of Fluids,* **30(3),** 722-731.

LEE, M.J. AND REYNOLDS, W.C. 1985 Numerical experiments on the structure of homogeneous turbulence . *Stanford University Report TF-24.*

ROGERS, M.M., MOIN, P. AND REYNOLDS, W.C. 1986 The structure and modeling of the hydrodynamic and passive scalar fields in homogeneous turbulent shear flow . *Stanford University Report TF-25.*

ROGALLO, R.S. 1981 Numerical experiments in homogeneous turbulence . *NASA TM 81315.*

SCHIESTEL, R. 1986 *C.R. Academy of Science, Paris.* **t. 302, ser II, no.11,** 727-730.

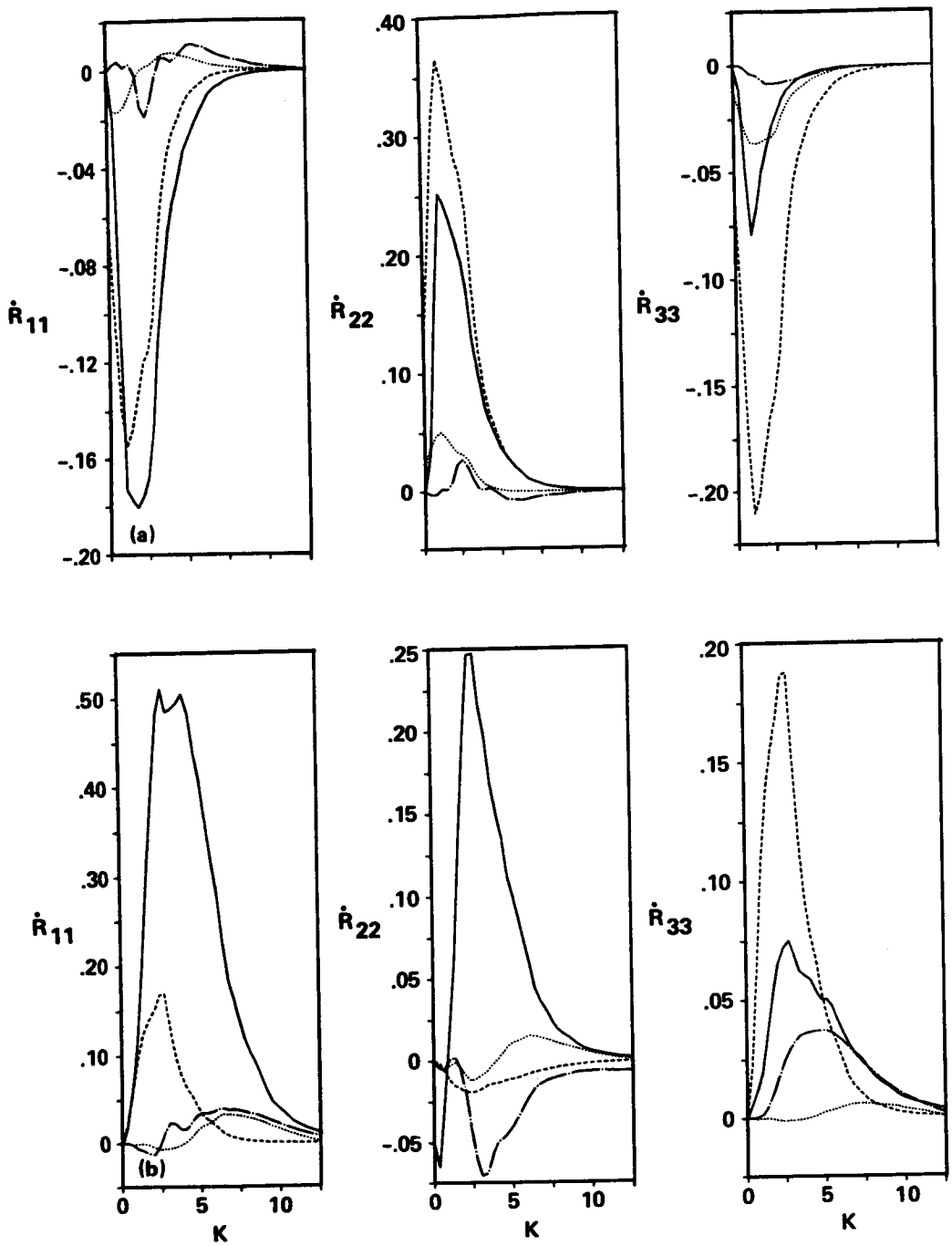

FIGURE 4. Homogeneous turbulence subjected to plane strain. Case PXB4 is shown. Evaluation of models for the pressure-strain and transfer terms. (a): pressure-strain, fast part; —— data, - - - - model (4), slow part; — · — data, ····· model (5). (b): transfer, fast part; —— data, - - - - model (9), slow part; — · — data, ····· model (8).

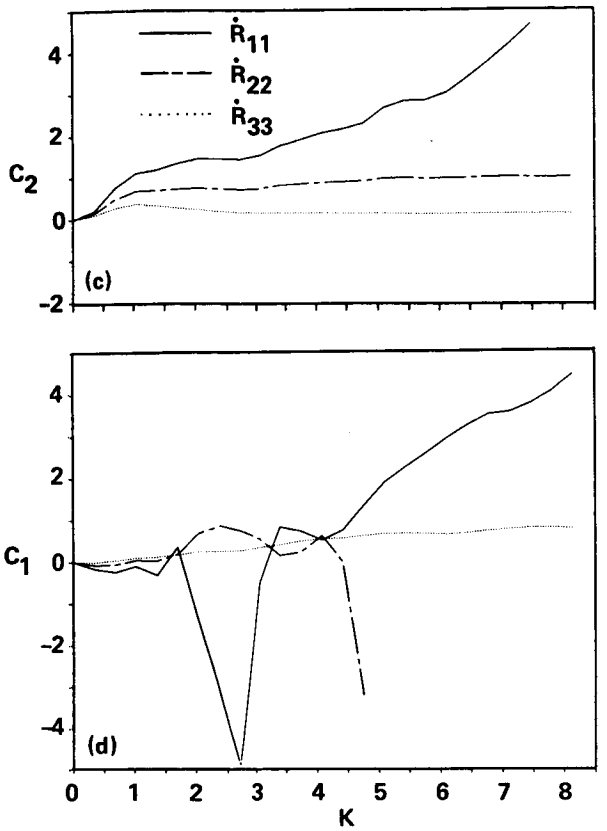

FIGURE 4 (CONCLUDED). Variation of the pressure-strain model coefficient for each component of R_{ij}: (c) fast part, (d) slow part.

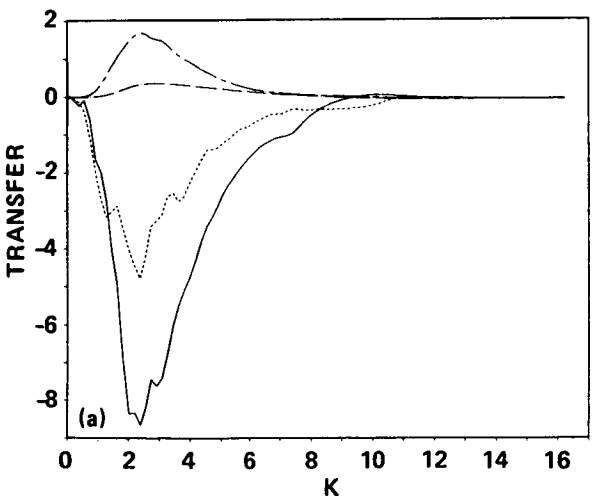

FIGURE 5. Homogeneous turbulence subjected to complex strains. Case M2V1 is shown. (a): gross energy transfer, fast part; —— data, - - - - model (7), slow part; —·— data, — — — model (6).

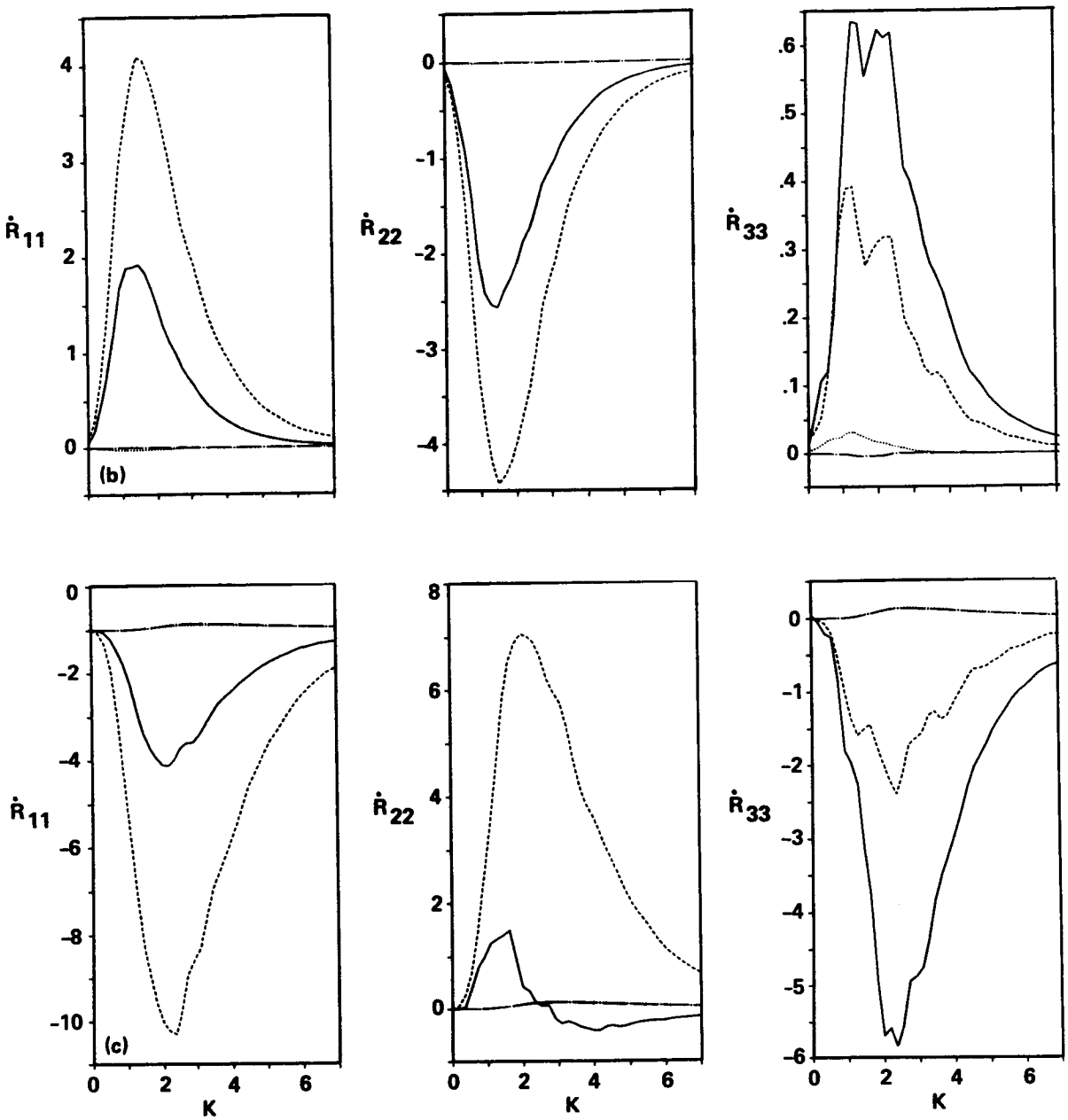

FIGURE 5 (CONTINUED). Evaluation of models for the pressure-strain and transfer terms. (b): pressure-strain, fast part; —— data, ---- model (4), slow part; —·— data, ····· model (5). (c): transfer, fast part; —— data, ---- model (9), slow part; —·— data, ····· model (8).

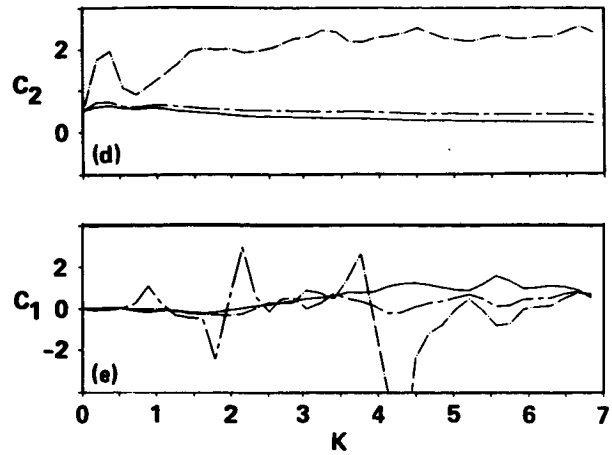

FIGURE 5 (CONCLUDED). Variation of the pressure-strain model coefficient for each component of R_{ij}: (d) fast part, (e) slow part. —— R_{11} term, — - — R_{22} term, — · — R_{33} term.

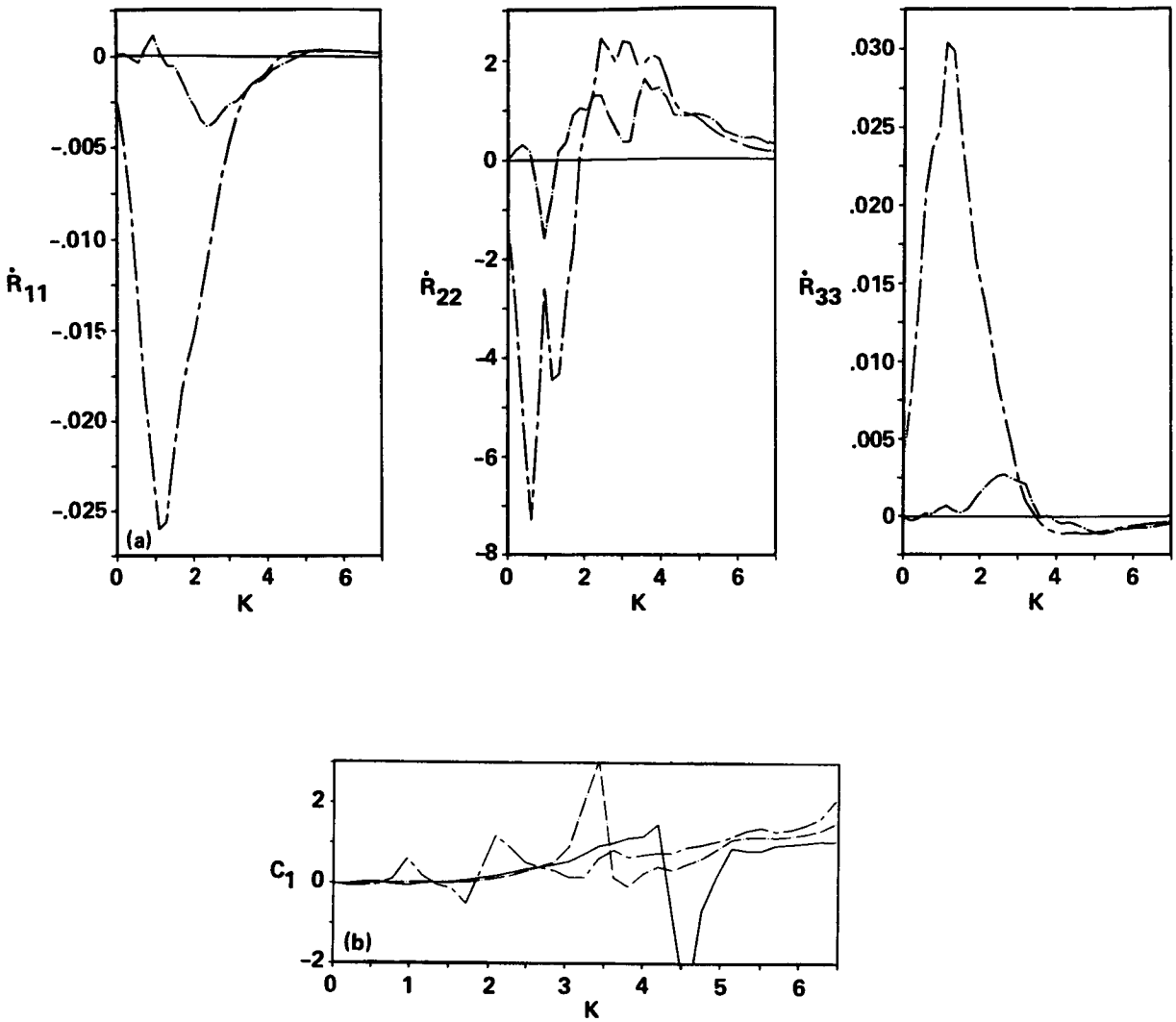

FIGURE 6. Relaxation of homogeneous turbulence subjected to complex strains. Case M2V1R1 is shown. (a): Slow pressure-strain; — · — data, — - — model (5). (b): Variation of the slow pressure-strain model coefficient for each component of R_{ij}: —— R_{11} term, — - — R_{22} term, — · — R_{33} term.